EELS analysis of Nylon 6 nanofibers reinforced with nitroxide-functionalized graphene oxide

César Leyva-Porras, C. Ornelas-Gutiérrez, M. Miki-Yoshida, Yazmín I. Avila-Vega, Javier Macossay, José Bonilla-Cruz.

Abstract

A detailed analysis by transmission electron microscopy (TEM) and electron energy loss spectroscopy (EELS) of nitroxide-functionalized graphene oxide layers (GOFT) dispersed in Nylon 6 nanofibers is reported herein. The functionalization and exfoliation process of graphite oxide to GOFT was confirmed by TEM using electron diffraction patterns (EDP), wherein 1–4 graphene layers of GOFT were observed. The distribution and alignment of GOFT layers within a sample of Nylon 6 nanofiber reveals that GOFT platelets are mainly within the fiber, but some were partially protruding from it. Furthermore, Nylon 6 nanofibers exhibited an average diameter of 225 nm with several microns in length. GOFT platelets embedded into the fiber, the pristine fiber, and amorphous carbon were analyzed by EELS where each spectra [corresponding to the carbon edge (C-K)] exhibited changes in the fine structure, allowing a clear distinction between: (i) GOFT single-layers, (ii) Nylon-6 nanofibers, and (iii) the carbon substrate. EELS analysis is presented here for the first time as a powerful tool to identify functionalized graphene single-layers (< 4 layers of GOFT) into a Nylon 6 nanofiber composite.

Introduction

Undoubtedly, since the graphene discovery by Novoselov et al. [1] using micromechanical exfoliation of graphite, an exponential increase in the amount of scientific and technological work has been observed, mainly due to their remarkable mechanical, thermal and electrical properties [2–5]. Graphene layers can be produced by chemical reaction of carbon precursors (bottom-up) e.g. chemical vapor deposition [6] or epitaxial growth [7]; and by exfoliation of graphite by (i) micromechanical exfoliation [1] or (ii) chemical treatment [8] (top-down). The graphite chemical processing to obtain graphene oxide (GO) using strong acids or other oxidizing compounds, and their subsequent intercalation/exfoliation and reduction, seems to be the most promising method to produce a single or a few graphene layers at large-scale, although this methodology includes several chemical steps. In particular, the functionalization of graphene or GO with chemical organic groups is the best way to achieve an effective dispersion or compatibility with a polymeric matrix, thus avoiding re-agglomeration or re-stacking of the fillers [9–12]. Nonetheless, the choice of functional groups, as well as the control of their concentration onto graphene oxide layers is crucial for the development of advanced materials with remarkable mechanical, physical and chemical properties, among others [11,12]. Therefore, several ingenious methodologies have been developed to modify the surface of graphite oxide flakes or layers of graphene oxide by attaching functional organic groups to increase their dispersability in common organic solvents, and thus achieve relatively good dispersions in a polymer matrix [11]. Recently, we have disclosed a simple approach to produce in one-step synthesis, single layers of graphene oxide decorated with nitroxide moieties (GOFT), using oxoammonium salts (halogen-nitroxide) as intercalating-reaction-

compatibilization agents under mild reaction conditions in order to functionalize the groups present on the surface and edges of graphite oxide and thus promote the exfoliation [12]. Hence, the improved properties can be directly correlated with both the exfoliation level and the dispersion degree, of graphene layers or graphene oxide into the polymeric phase.

On the other hand, detailed information on the graphene layers exfoliation (by measuring their interlayer distance), dispersion degree (quantifying the layers number) and the relative alignment of graphene or graphene oxide in polymeric matrices can be obtained by transmission electron microscopy (TEM) [13]. Nevertheless, the identification of graphene single-layers embedded within the polymer matrix is not trivial, since both materials are mainly formed of carbon atoms and consequently the contrast produced among them is very similar, so there is a very weak contrast. Thus, identification of two similar materials or phases by TEM is not straightforward and requires microscopes equipped with different configurations in the magnetic lenses and in the electron beam. In addition, the information acquired by TEM comes from a very small area of the sample [14] and frequently it is necessary to analyze several regions to get more representative results. As a consequence of these technical limitations, well-dispersed graphene single-layers or graphene oxide single- layers within a polymeric nanofiber have not been conclusively identified by TEM.

Electron energy loss spectroscopy (EELS) is an important characterization technique available in most of the transmission electron microscopes. In spite of its experimental complexity, EELS has been widely used to measure the sp^2 hybridizations characteristic on graphene [15]. The electron beam produces transitions in the sample

from the internal energy level 1s to unoccupied higher energy states. These excited states are known as r* and p* [16] and correspond to single and double bonds between carbon atoms, respectively. Thus, it is possible to know the conversion degree of CAC bonds to CAH bonds by quantifying the sp^2 hybridization. For instance, this phenomenon occurs during the oxidation and functionalization processes of natural graphite to obtain graphene oxide [17]. Also, EELS analysis has been applied to distinguish interfaces at low spatial resolutions and high elemental detection sensitivity, in order to observe hetero-interfaces, nanoscale mixing, and nanophase separation in polymeric matrices [18]. Specifically, in the composites field based on graphene/polymer, EELS analysis only has been used as a mapping tool; for example, Wang et al. [19] used EELS technique to establish the distribution of polyaniline on the surface of an individual graphene/polyaniline sheet, by detecting nitrogen signals from polyaniline.

To the best of our knowledge, the identification, distribution, and alignment of graphene single-layer or graphene oxide single-layer embedded within polymeric nanofibers has neither been observed nor analyzed in detail by TEM/EELS before. Hence, a detailed characterization by TEM/EELS analysis of a polymer composite based on nonwoven Nylon 6 nanofibers reinforced with graphene oxide layers decorated with nitroxide groups (GOFT) is presented herein for the first time. GOFT layers were observed and distinguished from the Nylon 6 nanofibers by scanning transmission electron microscopy (STEM). The images obtained undeniably reveal the presence of GOFT single-layer and a few layers inside the polymer fibers. In addition, the selected area electron diffraction patterns (SAED) showed the graphene fingerprint,

which demonstrates the success in the exfoliation/functionalization process to produce GOFT single-layer from graphite oxide. Finally, EELS analysis is presented in this manuscript as a powerful tool to identify GOFT single-layer of several layers of GOFT by using the characteristic core energy loss for carbon. Further, this technique was employed for correlating the thickness of the GOFT layers well-dispersed into a Nylon 6/GOFT composite. EELS allows making a clear distinction between: (i) nitroxide-functionalized graphene oxide (GOFT) single- layer, (ii) Nylon 6 nanofibers, and (iii) the carbon substrate, due to characteristic changes in their fine structure and intensity.

Experimental

Instrumentation:

TEM/EELS characterization was carried out using a high-resolution transmission electron microscope (HRTEM) JEOL JEM- 2200FS equipped with a spherical aberration corrector in the condenser lens and operated at an accelerating voltage of 200 kV. The identification and quantification of the elements from the functional groups was carried out by energy dispersive spectroscopy (EDS), using an INCA x-sight system from Oxford Instruments. EELS spectra were acquired in STEM mode using an in-column Omega filter system and a charge-couple device (CCD) detector with a resolution of 2024^2 pixels. The resolution of the EELS spectrum was 1.09 eV, calculated from the mean peak height of the zero loss peak. Low loss spectra were acquired at 0.2 s and core loss spectra at 5 s. Each spectrum represents the average of 10 acquisitions. The set of condenser aperture, slit width and entrance aperture were kept fixed during all experiments. The acquisition of all spectra was carried out during the same microscopy session, aligning the electron beam each time the sample was changed. Afterwards,

each acquired spectrum was corrected by subtracting the background signal. The plural scattering was removed by following the standard method of Fourier-ratio [20]. These steps were done employing the software Digital Micrograph version 1.53 from Gatan Inc.

Sample preparation:

A small amount of GOFT (nitroxide-functionalized graphene oxide single-layers) and composite Nylon 6/GOFT nanofibers (GOFT = 0.1 wt.%) were dispersed in absolute alcohol using an ultrasonic bath. Subsequently, a drop of the sonicated dispersion was dripped on a 3 mm copper grid covered with a holey carbon film. Finally, to remove the remaining alcohol in the sample, the copper grid containing the sample was dried under a lamp of 100W for 1 h.

Functionalization and exfoliation of graphite oxide with TEMPO moieties and composite based on Nylon-6/GOFT:

The detailed procedure of synthesis and characterization of GOFT, and the procedure to obtain nanofibers composites of Nylon6/GOFT by electrospinning have been previously described by our work group [12]. Briefly, the exfoliation and functionalization reaction of graphite oxide to obtain graphene oxide single-layers functionalized with TEMPO groups (GOFT) in the presence of Br-TEMPO (oxoammonium salt) was performed in a glass reactor equipped with a cooling jacket, a condenser and a magnetic stirrer. To obtain GOFT, 0.5 g of graphite oxide (which was previously obtained using an improved Hummer's method) was placed into the glass reactor in the presence of 2.6 g (0.025 mol) of trimethylamine and 60 mL of N-N-

dimethylformamide (DMF was used to improve the graphite oxide dispersion). The dispersion was sonicated during 30 min at 150W. Then, the dispersion was vigorously stirred and a solution of 2.5 g of Br-TEMPO (0.010 mol) in 40 mL of DMF was added dropwise [21,22]. The reaction was carried out at 2 °C under a N_2 atmosphere during 4 h. Functionalized and exfoliated graphene oxide layers with nitroxide moieties (GOFT) were washed with fresh DMF and filtered using a Nylon membrane of 0.2 lm under vacuum, followed by drying overnight at room temperature.

Preparation of polymer-GOFT dispersions by electrospinning: A 7.5 wt.% Nylon 6 solution was prepared by dissolving the polymer overnight in 1,1,1,3,3,3-hexaflouro-2-propanol (HFIP). The polymer-GOFT dispersions were prepared by placing 0.1 wt.% (with respect to the polymer) of GOFT in the Nylon 6/HFIP solution, and sonicated using the ultrasonic processor operating at 20 kHz with amplitude of 20% for 1 h in an ice bath to avoid excessive heat generated during the process, affording a black-ink like appearance dispersion. The polymer-GOFT dispersion were electrospun with an applied voltage of +15 kV in the needle tip, while the negative electrode was set to a voltage of -15 kVin the collector. A 15 cm distance between the needle tip and the rotating collector wasused to obtain the nanofibers, which were dried under vacuum for 24 h in the presence of P_2O_5 for removing any traces of residual moisture and solvents.

Results and discussion

Functionalization of GO with nitroxide groups:

Although the structure of graphene oxide is still uncertain [17,23], the presence of functional groups (OH, COOH, C=O and CAOAC) along their surface and edges is

reasonably accepted [17,24]. In addition, the molar concentration of these functional groups and their distribution strongly depends on the oxidation pathway used [24–26].

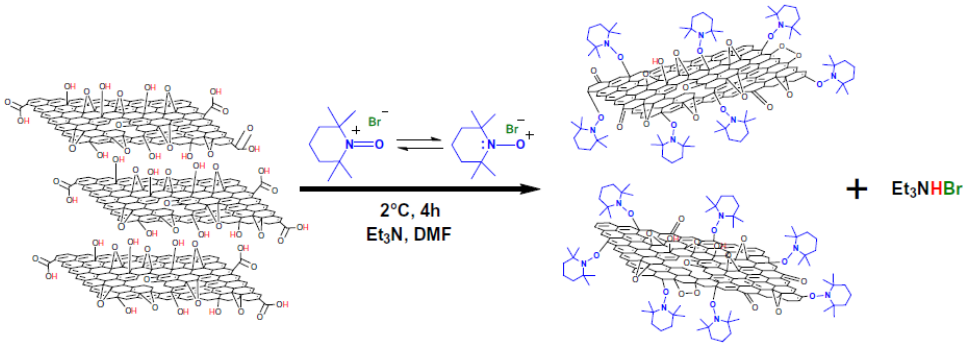

Fig. 1 – Exfoliation and functionalization of GO with nitroxide moieties using oxoammonium salts. Schematic representation. (A colour version of this figure can be viewed online.)

A detailed functionalization/exfoliation mechanism of graphite oxide to produce nitroxide-functionalized graphene oxide (GOFT) using oxoammonium salts has been previously reported by our group [12].We proposed that the protons in aromatic alcohol and acid moieties presented on the surface and edges of GO, should be first abstracted by an excess of Et3N, [27,28] as shown in Fig. 1, resulting in phenoxides and carboxylates [27], which then react with the 2,2,6,6,tetramethylpiperidine- 1-oxoniumcation to yield different functional groups [12].

Furthermore, phenols are known to oxidize under free radical conditions [29] and the nitroxide itself is a free radical [30], so we proposed that the material obtained consists of graphene oxide with several functional groups and alkoxyamine species attached to it. Meanwhile, the bromine anion is capped with Et3NH+ forming a white precipitate, indicating that the reaction has taken place. Hence, the reaction with

nitroxide seems to promote a re-oxidation of graphite oxide and a simultaneous exfoliation, as represented in Fig. 1.

GOFT characterization:

Fig. 2 shows the results from TEM analysis. Fig. 2A shows a bright field TEM image of a GOFT single-layer. The dimensions of the layer are approximately 0.8 lm· 0.2 lm, where a bend-like surface and some regions with imperfections and holes can be appreciated. We believe that the defects observed arose from the oxidation-functionalization process, which is in agreement with the data obtained from EDS analysis (not shown in the figure) wherein the oxygen concentration in natural graphite is below 1 wt.%, while for GOFT was above 15 wt.%. The dark tiny dots on the surface of the layer give a granular type appearance.

Hence, these imperfections should correspond to the addition of the different functional groups formed during the functionalization/exfoliation of graphite oxide. In addition, the layer edges exhibit imperfections, so there are regions where the edges are rounded or deformed, and this is also a consequence of the oxidation and functionalization process. Furthermore, the platelet in Fig. 2A is observed as a very thin material, since its contrast is weaker in comparison with the carbon grid membrane (during the image acquisition the contrast was enhanced using an omega filter and the carbon membranes deposited on the grid have a thickness of about 5–10 nm).

Fig. 2B shows a higher magnification image from both, the surface and the edge on a thicker GOFT layer. The image shows that the attached functional groups are well distributed on the GOFT surface and this was observed on both, the surface and the

edges. Li et al. [31] observed and attributed this effect to the breakdown of the conjugation in the plane of graphite due to: (i) the loss of carbon atoms during the oxidation process of natural graphite; and (ii) to the attachment of numerous functional groups chemically bonded to the surface and edges. Additionally, these functional groups weaken the van derWaals interactions between the graphite oxide layers, making it possible their exfoliation in single-layers [32]. Following the strategy reported by Meyer et al. [33], was possible to qualitatively determine the number of the GOFT layers. They proposed a simple way to identify and characterize a graphene single-layer from graphene multilayer (two or more layers) by simulations of the electron diffraction pattern (EDP) and the interpretation of the structure factor. According to this method, after a graphene single-layer is localized, an EDP is acquired. By comparison of the intensities of the diffracted planes, those closer to the direct beam (central beam) should be more intense than those more distant. When shifting the Ewald sphere (tilting the sample), for a graphene single-layer the difference in the intensities remains almost constant. Meanwhile for graphene multilayer, the difference in the intensities varies in a modulated way. These variations in the intensities are caused by the differences in the structure factor between the graphene single-layer and the multilayer. Thus, by using the diffraction pattern and plotting the intensity profile along a straight line, as shown in Fig. 2C and D, respectively; it is possible to affirm that the structure shown in Fig. 2A corresponds to a graphene single-layer. The amorphous zones observed in the EDP as a blur, is an effect produced by the functional groups chemically linked to the GOFT single-layer, which are certainly amorphous in nature. Nevertheless, although these results indicate the functionalization/exfoliation of graphite oxide to GOFT single-layers,

we also found some layers formed with less than 10 GOFT layers, which suggest that the efficiency of the functionalization/exfoliation reaction is slightly lesser to 100%.

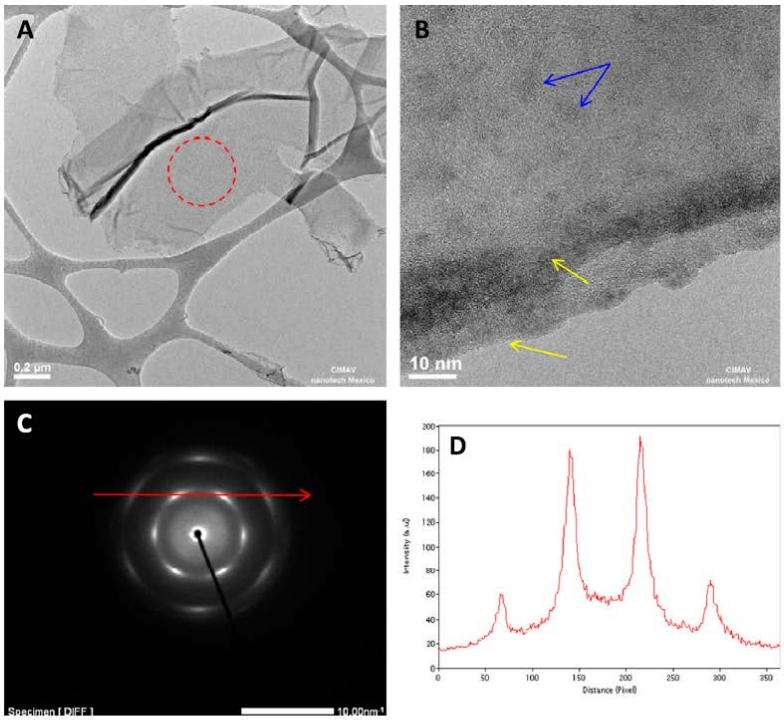

Fig. 2 – (A) TEM image showing a GOFT single-layer. The dotted red circle shows the region where the diffraction pattern was acquired. (B) Higher magnification TEM image from a thicker GOFT. Top arrows (blue) indicate the attached functional groups on the surface, while bottom arrows (yellow) show those attached on the edges. (C) Selected area electron diffraction pattern (SAED) from image 2A. The red arrow shows the direction of the intensity profile in (D). (A colour version of this figure can be viewed online.)

Polymer composite characterization:

Fig. 3 shows several images from a single Nylon 6 nanofiber and the composite nanofiber. In Fig. 3A, a bright field TEM image of a pristine Nylon 6 nanofiber is shown. The average diameter of the fibers was determined to be 225.8 ± 69 nm. The lengths of the fibers obtained from electrospinning are usually in the range of microns to several tens of microns [34]. The inset in the image shows an SAED pattern acquired from the indicated zone. This pattern shows a serial of diffuse rings, which are characteristic of the short-range order structure in the fiber. It is known that polymers, such as Nylon 6

are semi-crystalline in nature [35], and these polymers present segments randomly accommodated and segments with a short-range order. In our case, the crystallinity was not detected in the EDP since the percentage of crystallinity in the polymer was very low. Additionally, since both Nylon 6 and GOFT platelets are carbon-based materials, the contrast difference was weak.

Thus, using bright field images in any operating mode (TEM or STEM) to identify and differentiate the two structures in the composite was not a straightforward task. For this reason, and for this kind of composites, it is preferred to use a high angle annular dark field (HAADF) detector in STEM mode, which is known as Z-contrast configuration. The advantage of this technique relies in that, small differences in the average atomic number or thickness of the material are observed with a higher contrast difference in the dark field image [36]. Fig. 3B shows a Z-contrast image with two composite nanofibers positioned almost perpendicular to each other. On the lower surface of the horizontal

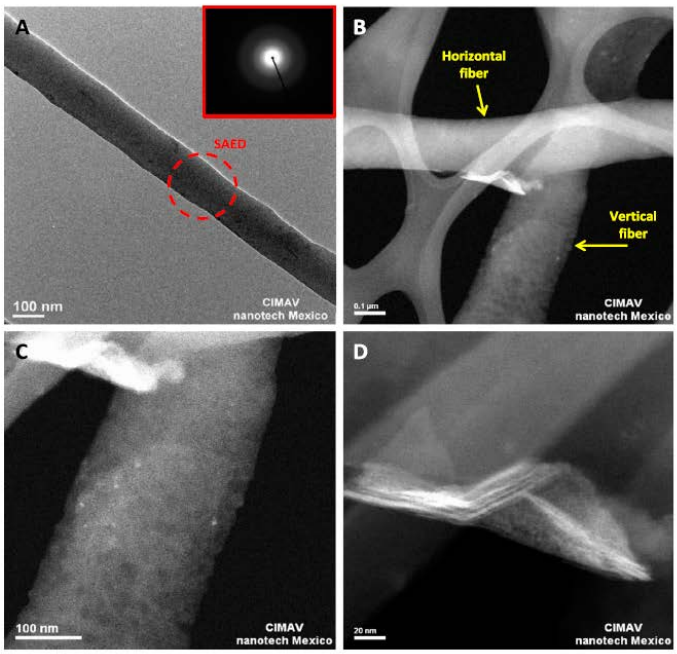

Fig. 3 – (A) TEM bright field image. The inset shows the SAED acquired in the circumscribed region by the red dotted circle. (B) STEM Z-contrast image showing two fibers containing GOFT layers. Arrows indicate the horizontal and vertical fibers. Higher magnification Z-contrast images from: (C) vertical fiber and (D) horizontal fiber. (A colour version of this figure can be viewed online.)

fiber, an irregular shape platelet was observed, whereas in the vertical fiber, a rectangular particle with very weak contrast was detected. We believe that in both cases, these features correspond to GOFT layers added to the polymer dispersions prior to electrospinning and therefore fiber formation. Higher magnification images are shown in Fig. 3C and D. For the case of the vertical fiber (Fig. 3C), the dimensions of the particle are approximately 165 nm · 190 nm. Both, size and morphology correspond to the GOFT layers previously characterized. Moreover, the fact that the contrast of the particle is tooweak, which is hardly distinguishable, suggests that the particle corresponds to a very thin GOFT layer that seems to be located inside of the fiber. On the other hand, the platelet in Fig. 3D shows a stronger contrast and seems to be made of four folded layers [37].

One aspect which we consider important to note, is that In this experiment we did not observe any type of carbonaceous spider wave-like structure similar to the one reported by Pan et al. [38]. These authors explained that the formation of this spider wave-like material was caused by the addition of graphene oxide into the polymer solution, and by further degradation of the Nylon 6 nanofiber due to the use of formic acid as the electrospinning solvent. Furthermore, it was also suggested that two effects caused reinforcement in the nanofiber, the hydrogen bonding interaction between the fiber, and the graphene oxide sheets that promoted the interaction of the polymer fibers with the spider wave like structure.

From the evidence found in our studies, we propose that the GOFT layers were effectively dispersed in the polymer solutions prior to electrospinning, resulting in their incorporation and alignment within a polymeric nanofiber. However, some of these layers can protrude from one nanofiber and then continue into another neighbor nanofiber, behaving as crosslinking agents. In this work we used to functionalize/ exfoliate, a commercial graphite oxide [12], which has nonhomogeneous particle size distribution. We believe that the phenomenon of alignment and the fact that some layers protrude from the fiber, strongly depends on the thickness and size of the graphene layers incorporated, respectively; and this assumption is in good agreement with the literature. Recently, Wang et al. [39] observed the alignment effect of graphene oxide layers in epoxy/graphene oxide nanocomposites, by using three different particle size distribution of graphene oxide sheets. The best alignment as well as an improved toughness was obtained when a smaller size distribution (0.7 lm) of graphene oxide layers was used. Thus, GOFT single-layers with small size may be aligned within

polymer nanofiber, meanwhile agglomerates of GOFT with big size hardly could be aligned and then could protrude from the fiber.

Furthermore, based on the chemical nature of the amide bond in Nylon 6 and the different chemical groups present in GOFT, it is reasonable to believe that these two materials could establish chemical bonding to further enhance the macroscopic mechanical properties of the resulting composite, as it has been observed in our laboratory and will be disclosed in a next contribution.

EELS characterization

Fig. 4 shows STEM images taken from different zones on the sample where EELS spectra were acquired. These zones are properly identified in the STEM image by means of circles, squares and triangles. Fig. 4A shows a GOFT platelet. Besides the spectra acquired on the platelet, other spectra were taken on the amorphous carbon membrane. In addition, Fig. 4B illustrates the regions where EELS spectra were acquired for the GOFT platelet embedded into the composite nanofiber, as well as other regions corresponding to the single fiber. In this analysis, all spectra were treated in the same way as discussed in the Section 2.

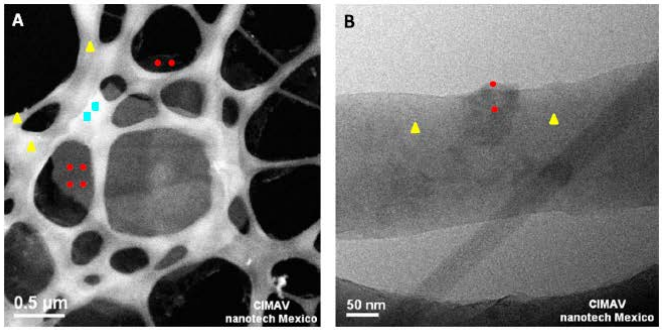

Fig. 4 – STEM images illustrating the areas where the EELS were acquired. (A) A few layers of GOFT platelet (less than 4). Circles (in red) correspond to the GOFT platelet, triangles (in yellow) to the amorphous carbon and squares (in cyan) to the platelet in contact with the amorphous carbon membrane. (B) Composite nanofiber containing a thicker GO platelet. Circles (in red) correspond to the GOFT platelet into the fiber and triangles (in yellow) to the single fiber. (A colour version of this figure can be viewed online.)

Normalized EELS spectra showing the carbon core-loss (C-K edge) is presented in Fig. 5. In this figure, it is possible to observe differences between the response intensity of the edges and the shape of the spectra curves. At an energy loss of 285 eV the 1s to π* transition is observed, while the states corresponding from 1s to p* transition were observed from 290 eV to about 330 eV [4].

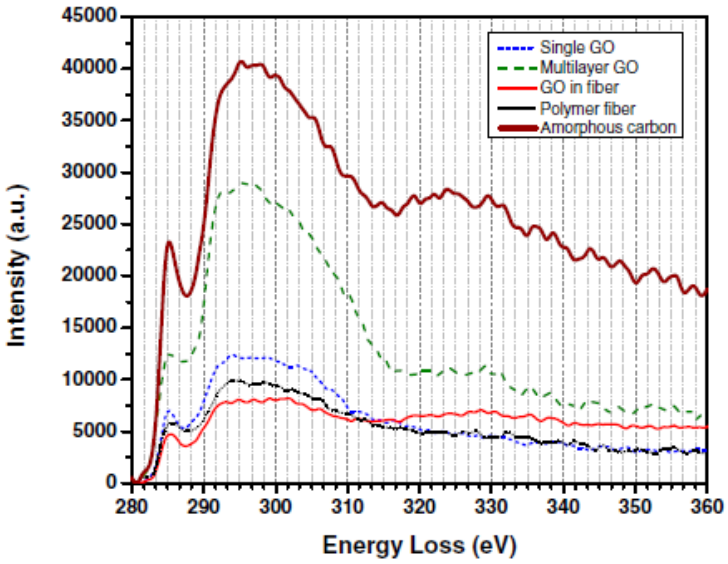

Fig. 5 – Carbon (C-K edge) core-loss EELS spectra acquired from the different samples. (A colour version of this figure can be viewed online.)

These transitions are the main features of the EELS spectra for graphite and other carbon-based materials and both correspond to the excitation fingerprint of the valence band electrons, above the Fermi level. Rosenberg et al. [41] identified several of such transitions and compared the experimental spectra with the theoretical density of states (DOS) for the highly oriented pyrolytic graphite (HOPG), assigning some of these peaks to the corresponding states identified in the specific Brillouin zones. Identification of the transitions in EELS spectra was done by carefully observing each of the spectrums. The only method employed during this task, were the background subtraction and the plural scattering removal (as stated in the Section 2). Once this procedure was applied, the spectra were observed as those presented in Fig. 5. From the detailed observation of each spectrum, after 290 eV it is possible to distinguish low-signal peaks. By comparing with those reported by Rosenberg et al. [41], it was realized that those low-signal peaks were not noisy-signal, but real transitions. After analyzing in detail each EELS spectrum for GOFT single-layer, GOFT multilayer, GOFT in nanofiber, Nylon 6 nanofiber and amorphous carbon, up to 8 transitions were found, which were identified and labeled from A to J. These transitions are shown in Table 1, where it is possible to observe that the energy peak of each transition (A–J) is very similar among the different samples, with the difference between them being less than 2 eV. Dato et al. [42] reported that the two main transitions in the core-loss spectra for a graphene single-layer and bi-layer present the same characteristics. Furthermore, Gass et al. [43] showed that the intensity of the spectrum in the low loss region (plasmon) increases directly with the number of graphene layers. On the other hand, Eberlein et al. [44] observed that unlike the plasmon, the high loss spectrum is not useful for distinguishing

different layers of graphene, since the edges corresponding to the transitions 1s to π* and 1s to σ* do not move to the left (redshift) as the number of graphene layers is decreased. Then, when observing the different characteristic states of the fine structure in our samples, we found that in general all presented the same signals. This is due to the similarity in the type of bonding, where the first and second neighboring carbon atoms are located at similar distances in both, graphite and amorphous carbon [45]. However, dissimilarities in the intensities and in the shape of the high loss spectra indicate differences between the samples, which are discussed herein.

In the specific case of the Nylon 6 nanofiber, it is observed that the edge at 286 eV (1s to π* transition) widens towards the high-energy loss region; this is caused by the loss of long range ordering as in a short-range order material, where the bonding is presented randomly in all directions [15]. When the Nylon 6 nanofiber spectrum is compared with the corresponding amorphous carbon spectrum, we found that the intensity of the spectrum for the nanofiber is much lower and that there is some reduction in the detail of the fine structure. These variations can be attributed to the differences in thickness between the two samples; as it is known that the intensity of the core edge decreases monotonically with increasing the sample thickness [46,47]. In this study, the nanofibers have an average diameter of 225 nm while that from the carbon membrane is smaller, in the order of 5– 10 nm. Hence, the intensity of the signal is lower for the nanofiber.

Furthermore, when comparing the spectra between the GOFT platelets with different number of layers, a single-layer presented a decrease in the intensity of the 1s to p* transition and a loss in the detail of the fine structure. The first effect is explained in

terms of electrons mobility; the electrons in the GOFT single-layer are restricted to move only in the plane of graphene, while increasing the number of graphene layers results in electrons moving between the layers [48]. Accordingly, the increase in electronic interactions among the layers is responsible for the increase in the detail of the fine structure [49]. This is corroborated when observing a feature from the fine structure in the multilayer GOFT. Approximately at 40–50 eV after the C-K edge, there is an increase in the signal, which is known as σ* dispersion. This signal belongs to the dispersion from the second layer, and in the graphite corresponds to the sixth nearest neighboring atoms in the ab plane [50].

Table 1 – Transitions found in this work for each sample analyzed by EELS. Values reported by Rosenberg et al. [41] for HOPG are listed at the end of the table for comparison purposes.

Sample	Peak energy (eV)									
	A	B	C	D	E	F	G	H	I	J
Single layer GOFT	284.8	291.8	293.4	298.3	302.7	307.4	310.7	316	329	333
Multilayer GOFT	284.9	292.1	294.4	299.3	304	308.1	309.8	315.8	328	334
GOFT in fiber	284.8	291.5	294	296	301	307	310	316.5	327	334
Polymer fiber	285	291.9	296.6	297.5	301	305.7	310.1	325.6	327	331
Amorphous C	285.4	292.5	294	297	304	307	310	316.7	328	334
Rosenberg et al. [41]	285.5	292.5	295.5	297.8	303.5	307.5	308.5	316.5	329	333

After identifying all these features in the different spectra, we can correlate the EELS spectra corresponding to the GOFT platelet within the Nylon 6 nanofiber. Evidently, the electron beam passes through the fiber and the GOFT platelet, obtaining a spectrum with the characteristics of both materials. The 1s to π* transition becomes wider, resembling that from the single Nylon 6 fiber. The intensity of the spectra for the GOFT in the nanofiber is less than for the GOFT single-layer, and even less that for the single Nylon 6 nanofiber. As discussed above, this effect is caused by the increase in the thickness of the sample, since in this case the electron beam has to pass through the fiber and the GOFT layers. The decrease in the detail of the peaks between 291 and

314 eV suggests a reduction in the number of layers in the GOFT platelet. Finally, the increase in the signal at 330 eV is similar to that found in the multilayer platelet, but different to the signal found in the fiber. Certainly, it is not possible to accurately determine the number of graphene sheets in the GOFT platelet within the Nylon 6 fiber. However, when comparing the EELS spectrum of the samples, the spectrum from the GOFT within the Nylon 6 fiber exhibits similar features, with those from the Nylon 6 fiber, GOFT single layer and GOFT multilayer. A fact derived from the results of exfoliation (Section 3.2), was the great abundance of GOFT platelets less than 10 layers. Consequently, it was easier to find thin GOFT platelets within the Nylon 6 fibers. These observations allow us to conclude that the GOFT platelet was located within the polymer nanofiber and the thickness of the platelet was less than 4 layers of GOFT.

Finally, since the intensity of the edge transition (C-K) is sensitive to the relative orientation between the electron beam and the sample, the differences between these transitions depend on the incidence angle (a) drawn among the electron beam and the surface of the sample. That is, as a increases, the intensity of the 1s to π* transition increases linearly. Therefore, to validate our spectra and adequately compare them, it is necessary to ensure that there are no variations in the angle of incidence. After comparing our spectra with the spectra reported by Rosenberg et al. [41], and determining the intensities ratio from the two main transitions (π*/σ*), it is possible to conclude that the angle of incidence for most of the samples is very close to 30°. Only the spectrum obtained from the multilayer GOFT presented an incidence angle of approximately 25°. Our experiments did not involve a variation in the angle of incidence and once the electron beam was aligned, the tilt was kept constant during the analysis.

Therefore, it is clear that the slight variation in the tilt is due to the orientation of the sample relative to the electron beam.

Conclusion

The identification of the distribution and alignment of nitroxide- functionalized graphene oxide layers (GOFT) dispersed in Nylon 6 nanofibers has been achieved through transmission electron microscopy TEM/EELS. The functionalization and exfoliation process of graphite oxide to GOFT was also confirmed by TEM, wherein 1–4 graphene layers of GOFTwere observed. GOFT layers were found inside the electrospun Nylon 6 nanofibers, and in some cases, the layers are fully embedded within the polymer fiber, while in other cases the material protrudes from the fiber. Based on these observations, a simple reinforcement mechanism was proposed. EELS analysis is presented here for the first time as a powerful tool to identify functionalized graphene single-layers (<4 layers of GOFT) into a Nylon 6 nanofiber composite. From the EELS analysis, small details in the fine structure (characteristic of these materials) were observed, allowing to make a clear distinction between: (i) functionalized graphene oxide single-layers, (ii) Nylon 6 nanofibers, and (iii) the carbon substrate.

Acknowledgements

The authors thank to the Laboratorio Nacional de Nanotecnología (Nanotech) for the use of the HRTEM. A grant (#84322) from CONACYT-México for the support of this research is gratefully acknowledged. Also, this work was partially supported by NIH-NIGMS-NIA Grant #1SC2AG036825-01, for which J.M. is grateful.

References

[1] Novoselov KS, Geim AK, Morozov SV, Jiang D, Zhang Y, Dubonos SV, et al. Electric field effect in atomically thin carbon films. Science 2004;306(5696):666–9.

[2] Park S, Ruoff RS. Chemical methods for the production of

graphenes. Nat Nanotechnol 2009;4(4):217–24.

[3] Lee C, Wei X, Kysar JW, Hone J. Measurement of the elastic properties and intrinsic strength of monolayer graphene. Science 2008;321(5887):385–8.

[4] Balandin AA. Thermal properties of graphene and nanostructured carbon materials. Nat Mater 2011;10(8):569–81.

[5] Gomes KK, Mar W, Ko W, Guinea F, Manoharan HC. Designer

Dirac fermions and topological phases in molecular graphene. Nature 2012;483(7389):306–10.

[6] Xu SC, Man BY, Jiang SZ, Chen CS, Yang C, Liu M, et al. Direct

synthesis of graphene on SiO2 substrates by chemical vapor deposition. CrystEngComm 2013;15(10):1840–4.

[7] Maeda F, Hibino H. Molecular beam epitaxial growth of graphene using cracked ethylene—advantage over ethanol in growth. Diamond Relat Mater 2013;34:84–8.

[8] Park J, Yan M. Covalent functionalization of graphene with reactive intermediates. Acc Chem Res 2013;46(1):181–9.

[9] Kim H, Abdala AA, Macosko CW. Graphene/polymer nanocomposites. Macromolecules 2010;43(16):6515–30.

[10] Khan U, May P, O'Neill A, Coleman JN. Development of stiff, strong, yet tough composites by the addition of solvent exfoliated graphene to polyurethane. Carbon 2010;48(14):4035–41.

[11] Georgakilas V, Otyepka M, Bourlinos AB, Chandra V, Kim N, Kemp KC, et al. Functionalization of graphene: covalent and non-covalent approaches, derivatives and applications. Chem Rev 2012;112(11):6156–214.

[12] Avila-Vega YI, Leyva-Porras CC, Mireles M, Quevedo-Lo´pez M, Macossay J, Bonilla-Cruz J. Nitroxide-functionalized graphene oxide from graphite oxide. Carbon 2013;63:376–89.

[13] Soldano C, Mahmood A, Dujardin E. Production, properties and potential of graphene. Carbon 2010;48(8):2127–50.

[14] Kim H, Macosko CW. Morphology and properties of polyester/exfoliated graphite nanocomposites. Macromolecules 2008;41(9):3317–27.

[15] Berger SD, McKenzie DR, Martin PJ. EELS analysis of vacuum arc-deposited diamond-like films. Philos Mag Lett 1988;57(6):285–90.

[16] Bernier N, Bocquet F, Allouche A, Saikaly W, Brosset C, Thibault J, et al. A methodology to optimize the quantification of sp2 carbon fraction from K edge EELS spectra. J Electron Spectrosc Relat Phenom 2008;164(1–3):34–43.

[17] Dreyer DR, Park S, Bielawski CW, Ruoff RS. The chemistry of graphene oxide. Chem Soc Rev 2010;39(1):228–40.

[18] Dehonor M, Lopez-Barro´n C, Macosko CW. Handbook of polymer synthesis, characterization, and processing. Chapter

20: Microscopy. John Wiley and Sons; 2013. pp. 409–421.

[19] Wang D, Li F, Zhao J, RenW, Chen Z, Tan J, et al. Fabrication of graphene/polyaniline composite paper via in situ anodic

electropolymerization for high-performance flexible electrode. ACS Nano 2009;3(7):1745–52.

[20] Egerton RF. Electron energy-loss spectroscopy in the electron microscope. third ed. New York: Springer; 2011.

[21] Bonilla-Cruz J, Lara-Ceniceros T, Saldı´var-Guerra E, Jime´nez-

Regalado E. Towards controlled graft polymerization of poly[styrene-co-(maleic anhydride)] on functionalized silica mediated by oxoaminium bromide salt. Facile synthetic pathway using nitroxide chemistry. Macromol Rapid

Commun 2007;28(13):1397–403.

[22] Bonilla-Cruz J, Lara-Ceniceros TE, Ramírez-Wong DG,

Saldívar-Guerra E, Pe´rez-Rodríguez F, Márquez-Lamas U. Amphiphilic block copolymer from hydroxyl-terminated polymers functionalized with TEMPO. A new synthetic method using oxoammonium salt. Macromol Chem Phys

2011;212(15):1654–62.

[23] Lu N, Yin D, Li Z, Yang J. Structure of graphene oxide: thermodynamics versus kinetics. J Phys Chem C 2011;115(24):11991–5.

[24] Marcano DC, Kosynkin DV, Berlin JM, Sinitskii A, Sun Z,

Slesarev A, et al. Improved synthesis of graphene oxide. ACS

Nano 2010;4(8):4806–14.

[25] Shen J, Hu Y, Shi M, Lu X, Qin C, Li C, et al. Fast and facile preparation of graphene oxide and reduced graphene oxide nanoplatelets. Chem Mater 2009;21(15):3514–20.

[26] Hummers Jr WS, Offeman RE. Preparation of graphitic oxide. J

Am Chem Soc 1958;80(6):1339.

[27] Bailey WF, Bobbitt JM, Wiberg KB. Mechanism of the oxidation of alcohols by oxoammonium cations. J Org Chem 2007;72(12):4504–9.

[28] Prucker O, Ru¨ he J. Polymer layers through self-assembled monolayers of initiators. Langmuir 1998;14(24):6893–8.

[29] Tebben L, Studer A. Nitroxides: applications in synthesis and

in polymer chemistry. Angew Chem Int Ed 2011;50(22):5034–68.

[30] Grubbs RB. Nitroxide-mediated radical polymerization: limitations and versatility. Polym Rev 2011;51(2):104–37.

[31] Li X, Zhang G, Bai X, Sun X, Wang X, Wang E, et al. Highly conducting graphene sheets and Langmuir–Blodgett films. Nat Nanotechnol 2008;3(9):538–42.

[32] Wang M, Liu Q, Sun H, Stach EA, Zhang H, Stanciu L, et al. Preparation of high-surface-area carbon nanoparticle/ graphene composites. Carbon 2012;50(10):3845–53.

[33] Meyer JC, Geim AK, Katsnelson MI, Novoselov KS, Obergfell D, Roth S, et al. On the roughness of single- and bi-layer graphene membranes. Solid State Commun 2007;143(1–2):101–9.

[34] Greiner A, Wendorff JH. Electrospinning: a fascinating method for the preparation of ultrathin fibers. Angew Chem Int Ed 2007;46(30):5670–703.

[35] Jia Z, Zeng F, Yuan Q, Misra RDK. Carbon nanotube-induced structure and phase evolution in polymer-based nanocomposites crystallized at elevated pressures. Mater Sci Eng, B 2012;177(9):666–72.

[36] Browning ND, Chisholm MF, Pennycook SJ. Atomic-resolution chemical analysis using a scanning transmission electron microscope. Nature 1993;366(6451):143–6.

[37] Cupolillo A, Ligato N, Caputi LS. Two-dimensional character of the interface-p plasmon in epitaxial graphene on Ni(1 1 1). Carbon 2012;50(7):2588–91.

[38] Pant HR, Park CH, Tijing LD, Amarjargal A, Lee D, Kim CS. Bimodal fiber diameter distributed graphene oxide/nylon-6 composite nanofibrous mats via electrospinning. Colloids Surf, A 2012;407:121–5.

[39] Wang X, Jin J, Song M. An investigation of the mechanism of graphene toughening epoxy. Carbon 2013;65:324–33. [40] Ponsonnet L, Donnet C, Varlot K, Martin JM, Grill

A, Patel V. EELS analysis of hydrogenated diamond-like carbon films. Thin Solid Films 1998;319(1–2):97–100.

[41] Rosenberg RA, Love PJ, Rehn V. Polarization-dependent C(K) near-edge x-ray-absorption fine structure of graphite. Phys Rev B 1986;33(6):4034–7.

[42] Dato A, Radmilovic V, Lee Z, Phillips J, Frenklach M. Substrate-free gas-phase synthesis of graphene sheets. Nano Lett 2008;8(7):2012–6.

[43] Gass MH, Bangert U, Bleloch AL, Wang P, Nair RR, Geim AK. Free-standing graphene at atomic resolution. Nat Nanotechnol 2008;3(11):676–81.

[44] Eberlein T, Bangert U, Nair RR, Jones R, Gass M, Bleloch AL, et al. Plasmon spectroscopy of free-standing graphene films. Phys Rev B 2008;77(23):233406–9.

[45] Duarte-Moller A, Espinosa-Magan˜ a F, Martı´nez-Sanchez R, Avalos-Borja M, Hirata GA, Cota-Araiza L. Study of different forms of carbon by analytical electron microscopy. J Electron Spectrosc Relat Phenom 1999;104(1–3):61–6. [46] Hosoi J, Oikawa T, Inoue M, Kokubo Y. Thickness dependence of signal/background ratio of inner-shell electron excitation loss in eels. Ultramicroscopy 1984;13(3):329–32.

[47] Cheng SC, Egerton RF. Elemental analysis of thick amorphous specimens by EELS. Micron 1993;24(3):251–6. [48] Yase K, Horiuchi S, Kyotani M, Yumura M, Uchida K, Ohshima S, et al. Angular-resolved EELS of a carbon nanotube. Thin Solid Films 1996;273(1–2):222–4. [49] Ste´phan O, Kociak M, Henrard L, Suenaga K, Gloter A, Tence´M, et al. Electron energy-loss spectroscopy on individual nanotubes. J Electron Spectrosc Relat Phenom 2001;114–116:209–17.

[50] Brydson R, Westwood AVK, Jiang X, Rowen SJ, Collins S, Lu S, et al. Investigating the distribution and bonding of light elements alloyed in carbonaceous materials using EELS in the TEM/STEM. Carbon 1998;36(7–8):1139–47.